

The stability of 30- μm -diameter water jet for jet-guided laser machining

Eddie Yin-Kwee Ng · Du Guannan

Received: 27 June 2014 / Accepted: 2 December 2014 / Published online: 23 December 2014
© Springer-Verlag London 2014

Abstract Combined water-jet process and laser machining, the water jet-guided laser processing is suitable in processing a thin and sensitive material with a high degree of precision required. Given that there are many uncertainties of the jet with lower than a 50- μm -diameter nozzle and lower velocities in the stability field of water jet-guided laser machining, a numerical model of a 30- μm water jet, considering the number of grids and the influence of meshes, has been studied to meet the requirements of micrometer order precision machining. Furthermore, the critical Reynolds number and the critical jet exit velocity of the case with a 30- μm -diameter nozzle have been presented to make a comparison between turbulence flow and laminar flow in air with different jet exit velocities from 0.2 to 500 m/s. Hence, the optimal jet exit velocity to achieve the longest stable length of water jet was found. Besides, three cases of 15 m/s jet exit velocity are simulated in different degrees of vacuum, which suggest water jets in vacuum are much more stable than those in atmospheric environment. Finally, a conjecture about water-jet simulation with a smaller diameter of nozzle is proposed as a future work.

Keywords CFD · Stability · Water jet-guided laser machining · Vacuum

1 Introduction

Conventionally, laser processing like CO_2 and Nd:YAG lasers are used in a variety of material processing applications for a wide range of materials, and there appears to be no limit to the

range of possible materials, which include metals, ceramics, composite materials, polymers, semiconductors, and biological tissue. However, it is difficult to position, control, track, and measure the focus precisely, and processing defects caused by positive and negative defocus are common and obvious; what is worse, burrs and V-grooving are inevitable when machining thick work-piece for the small range of laser focus and heat concentration [1].

In water jet-guided laser process (Fig. 1), the laser beam can be totally reflected on the wall of water jet and guided in the work-piece without taking the focus length into consideration. Thus, the working range is expanded dramatically; in the experimental research of Porter et al. [2], regardless of the variety of laser parameters, jet pressure, and nozzle diameter, the value of 50 mm was found to be a fairly reliable upper limit to the cutting distance for both normal and inclined surfaces [2]. Hence, the control of Z-axis is unnecessary, and V-grooving default can be eliminated by changing the distribution of heat fundamentally. Thus, work-pieces could be machined with high-dimensional accuracy and surface quality, especially in processing a thin and sensitive material [3–5].

Verifying those advantages of water jet-guided laser (WJGL) machining as in Table 1, some companies like Synova prefers to make high-performance WJGL machines. On the other hand, the numerical study of water jet-guided laser processing plays a significant role in optimizing equipment and manufacturing quality, such as modeling of water jet-guided laser grooving of silicon [1], drilling of silicon based on finite volume method (FVM) [6], clean dicing of compound semiconductors using the water jet-guided laser technology [7], heat damage-free laser-micro-jet cutting achieves highest die fracture strength [8], high-precision laser processing of sensitive materials by Micro-jet [9], and particle-free semiconductor cutting using the water jet-guided laser [10].

E. Y.-K. Ng (✉) · D. Guannan
College of Engineering, School of Mechanical and Production
Engineering, Nanyang Technological University, 50 Nanyang
Avenue, Singapore 639798, Singapore
e-mail: mykng@ntu.edu.sg

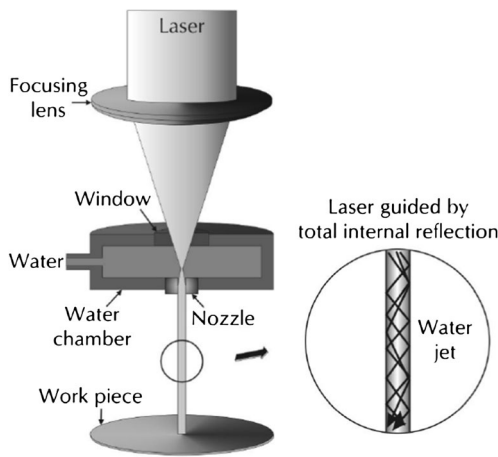


Fig. 1 The theories of water jet-guided laser (WJGL) machining [2]

Besides heat transfer and relative effect on work-piece [11–13], more scientists tend to focus on coupling mechanism and precision controlling in water jet-guided area. Given that the influence of nozzle geometry with different diameters, length-diameter ratios, and nozzle convergence angles are well studied in jet machining area, they prefer to deal with the stability parameters of water jet-guided laser machining, which has a dramatic effect on coupled laser quality, refer to the stability parameters and relative principles in jet machining field. Thus, the stability of water jet is considered rarely in water jet-guided laser machining field. Additionally, there appears to be no work reported for less than a 50- μm -diameter nozzle of water jet-guided laser machining. Furthermore, researchers [4, 11, 13] tend to use 150 to 250 m/s as the exit velocity in order to obtain higher kinetic energy, but Shanmugam D. K. have provided that an increase in the jet pressure decreased the jet stability in some cases [14]. Given that there are many uncertainties of the jet with

lower than a 50- μm -diameter nozzle and lower velocities, the simulation of a 30- μm -diameter nozzle with different velocities, including jet exit velocities lower than 150 m/s, is therefore the focus in this paper.

2 Numerical algorithm

Based on the breakup mechanism of jet [15–17], it is well accepted that the interaction between the air and jet results in breakage. In linear stability theory, the jet can be described as an elementary stream $U_0=U_0(r,\theta,z)$ with pressure p_0 and a small perturbation $U'=U'(r,\theta,z,t)$ with pressure p' .

Thus, the N-S equations are

$$\nabla \cdot U = 0$$

$$\frac{\partial U}{\partial t} + U \cdot \nabla U = -\nabla p + \frac{1}{Re} \cdot \nabla^2 U \tag{1}$$

where $U=U_0+\varepsilon U$, $p=p_0+\varepsilon p'$, ∇ as the gradient operator, ∇^2 as the Laplace operator, and $Re = \frac{\rho v d}{\mu}$ as the Reynolds number.

So we can get the jet disturbance equations

$$\nabla \cdot U' = 0$$

$$\begin{aligned} \frac{\partial U'}{\partial t} + U_0 \cdot \nabla U' + U' \cdot \nabla U_0 + \varepsilon \cdot U' \cdot \nabla U' \\ = -\nabla p' + \frac{1}{Re} \cdot \nabla^2 U' \end{aligned} \tag{2}$$

For initial perturbation, $U'=U'(r,\theta,z,t=0)$ whose disturbance energy is less than a constant value, as long as the size

Table 1 The comparison between conventional laser machining and WJGL machining [4]

	Conventional laser machining	WJGL machining
Wavelength of laser (nm)	1064 to 10,600	532 to 1064
Energy transfer mode	Optical fiber, galvanometer	Optical fiber, water jet
Processing power source	Solid state laser and gas laser	Solid state laser
Material removal methods	Laser, gas, thermal processing	Laser, water, cold processing
Working range (mm)	Range 0.5	Range 0–100
Z-axis tolerance	± 0.1 mm	No tolerance
The Z-axis control	Extremely sensitive and reliable	No Z-axis control
Replacement operations	Hard to replace the work-pieces	Easy to replace the work-pieces
Thickness (mm)	0.1–10	0.01–50
Minimum cutting width (mm)	0.15	0.017
Machining precision (mm)	0.05	0.001
Burrs and V-grooving	Inevitable	Rare burrs and V-grooving
Material thermal stress	Tempering, structure changed	No thermal stress
Smoke produced	Smoke is inevitable, toxic gases	Most smoke has been absorbed
Cutting waste	Waste materials exist as dusts	Water washed away waste

of its perturbations remain less than a given value ε , the same as $|U'|_{t \geq 0} < \varepsilon$, at all the times $t \geq 0$, the jet can be considered as stable. When it is small perturbations $\varepsilon \rightarrow 0$, we can obtain the linear perturbation equations:

$$\nabla \cdot U' = 0$$

$$\frac{\partial U'}{\partial t} + U_0 \cdot \nabla U' + U' \cdot \nabla U_0 = -\nabla p' + \frac{1}{Re} \cdot \nabla^2 U' \tag{3}$$

In cylindrical coordinates, assuming that the direction of the jet is opposite the Z-axis, the nozzle diameter is d , surface tension of gas-liquid interface is σ , jet kinematic viscosity is ν_1 , and pressure and density are respectively p_1 and ρ_1 . Kinematic viscosity and the pressure and density of the ambient air are ν_2, p_2 and ρ_2 , respectively. The initial state of jet is U_1 , the initial state of the air flow is U_2 , and the difference between jet pressure and the ambient air pressure $\Delta p = p_1 - p_2 = \frac{2\sigma}{d}$; thus,

$$\nabla \cdot U' = 0$$

$$\frac{\partial U'_j}{\partial t} + U_{0j} \cdot \nabla U'_j + U'_j \cdot \nabla U_{0j} = -\frac{\rho_1}{\rho_j} \nabla p'_j + \frac{1}{Re_j} \cdot \nabla^2 U'_j \tag{4}$$

Reynolds number Re , Weber number of intestinal We , and gas-liquid density ratio q are

$$Re_j = \frac{U_j d}{\nu_j}, We_j = \frac{\rho_j U_j^2 d}{\sigma}, q = \rho_2 / \rho_1 \tag{5}$$

where $j=1$ is referred to the liquid phase and $j=2$ is the ambient air.

Assuming that the gas-liquid interface suffers dimensionless perturbation:

$$\eta = \eta_0 \exp[\omega t + i(kz + m\theta)] \tag{6}$$

η_0 , the initial dimensionless perturbation amplitude, is related to the shape of the nozzle. Frequency $\omega = \omega_y + i\omega_i$ and wave vector $k = k_y + ik_i$, in which the subscript r respects the real number and the subscript i represents the imaginary number, ω_y represents the frequency of the disturbance wave, ω_i is the factor that determines perturbation amplitude varying with time, k_y represents the wave number, and k_i is the factor that determines perturbation amplitude varying with space. Real modulus m is the angular modulus, which represents the changes of disturbance wave of free surface at angle. When $m=0$, the amplitude of the disturbance is regardless of θ , and disturbances are in axisymmetric shape. When $m \neq 0$, the disturbances are in non-axisymmetric shape.

Suppose under the column coordinates the expression of (p'_j, U'_j) is

$$p'_j = p_{0j}'(r) \exp[\omega t + i(kz + m\theta)]$$

$$U'_j = U_{0j}'(r) \exp[\omega t + i(kz + m\theta)] \tag{7}$$

Put Eq. (7) into Eq. (4) and get

$$\begin{aligned} p_{0j}'(r) &= d_{j1} I_m(kr) + d_{j2} B_m(kr) \\ U_{0jr}'(r) &= a_{j1} I_m'(l_j r) + a_{j2} I_m(l_j r) + a_{j3} B_m'(l_j r) \\ &+ a_{j4} \frac{m}{l_j r} B_m'(l_j r) - \frac{Re_j k}{\lambda_j^2 Q_j} [d_{j1} I_m'(kr) + d_{j2} B_m'(kr)] U_{0jz}'(r) \\ &= i \left\{ a_{j1} \frac{l_j}{k} I_m(l_j r) + a_{j3} \frac{l_j}{k} B_m(l_j r) - \frac{Re_j m}{\lambda_j^2 Q_j r} [d_{j1} I_m(kr) + d_{j2} B_m(kr)] \right\} \\ U_{0j\theta}'(r) &= i \left\{ a_{j2} I_m'(l_j r) + a_{j1} \frac{m}{l_j r} I_m(l_j r) + a_{j4} B_m'(l_j r) \right. \\ &\left. + a_{j3} \frac{m}{l_j r} B_m(l_j r) - \frac{Re_j m}{\lambda_j^2 Q_j r} [d_{j1} I_m(kr) + d_{j2} B_m(kr)] \right\} \tag{8} \end{aligned}$$

where I_m and B_m are correction complex Bessel function, respectively. $\lambda_j^2 = Re_j(\omega - ik)$, $l_j^2 = k^2 + \lambda_j^2$, and $Q_1 = 1, Q_2 = q$.

The dimensionless boundary conditions of jet perturbation equations are

Kinematic boundary conditions:

$$U_{rj}' = \frac{\partial \eta}{\partial t} - \delta_{1j} \frac{\partial \eta}{\partial z} \tag{9}$$

in which $\delta_{11} = 1$ and $\delta_{12} = 0$

Dynamic boundary conditions:

$$\begin{aligned} p_1' - p_2' &= \frac{2}{Re_1} \frac{\partial U_{r1}'}{\partial r} - \frac{2q}{Re_2} \frac{\partial U_{r2}'}{\partial r} - \frac{q}{We_2} \left(\eta + \frac{\partial^2 \eta}{\partial z^2} + \frac{\partial^2 \eta}{\partial \theta^2} \right) \\ p_1' - p_2' &= \frac{2}{Re_1} \left(\frac{\partial U_{\theta 1}'}{\partial \theta} + U_{r1}' \right) - \frac{2q}{Re_2} \left(\frac{\partial U_{\theta 2}'}{\partial \theta} + U_{r2}' \right) \\ &- \frac{q}{We_2} \left(\eta + \frac{\partial^2 \eta}{\partial z^2} + \frac{\partial^2 \eta}{\partial \theta^2} \right) \frac{1}{Re_1} \left(\frac{\partial U_{z1}'}{\partial r} + \frac{\partial U_{r1}'}{\partial z} \right) \\ &- \frac{q}{Re_2} \left(\frac{\partial U_{z2}'}{\partial r} + \frac{\partial U_{r2}'}{\partial z} \right) = 0 \frac{1}{Re_1} \left(\frac{\partial U_{\theta 1}'}{\partial z} + \frac{\partial U_{z1}'}{\partial \theta} \right) \\ &- \frac{q}{Re_2} \left(\frac{\partial U_{\theta 2}'}{\partial z} + \frac{\partial U_{z2}'}{\partial \theta} \right) = 0 \frac{1}{Re_1} \left(\frac{\partial U_{r1}'}{\partial \theta} + \frac{\partial U_{\theta 1}'}{\partial r} - U_{\theta 1}' \right) \\ &- \frac{q}{Re_2} \left(\frac{\partial U_{r2}'}{\partial \theta} + \frac{\partial U_{\theta 2}'}{\partial r} - U_{\theta 2}' \right) = 0 \tag{10} \end{aligned}$$

According to the basic assumptions of the linear stability theory and the characteristics of the disturbance is growing as

time goes by, it is possible to develop into a real disturbance and cause the jet to break when the infinitesimal perturbations on the surface of the jet are accumulated for an unlimited long time. By the basic assumptions of Eq. (7) and the boundary conditions of Eqs. (9) and (10), we can obtain the equation of the disturbance characteristic of the jet and the impacts of Reynolds numbers Re , Weber number We , and gas-liquid density ρ on the stability of the jet. When the gas-liquid density ratio ρ is set, the undisturbed length LC when jet is stable can be expressed as

$$LC/d = CCWe_2^x Re_1^y \quad (11)$$

CC , related to the nozzle structure parameters and water pressure, is the jet breakup length coefficients; d is the diameter of the water jet (nozzle diameter); x and y are the index parameters; We_2 is Weber number of the surrounding gas; Re is water-jet Reynolds number; and We_2 and Re_1 are determined by the fluid density, fluid viscosity, jet velocity, diameter of nozzle hole, and the gas-liquid surface tension.

3 Model details

The exit plane diameter of nozzle D , which is the basis to determine other parameters, should be the first parameter to design. Considering water jet-guided laser processing should meet the requirements of ultra-precision machining, like wafer scribing process, the diameter of the nozzle should be as small as possible. However, the thinner water jet is (especially when $D < 50 \mu\text{m}$), the more difficult to achieve in labs [18, 19], so a 30- μm diameter has been selected in the present modeling (Fig. 2).

In previous researches, the length-diameter ratio is an important parameter that directly affects the flow resistance and flow coefficient [4]. Study shows that if the length-diameter ratio (L/D) is smaller than 2, this nozzle can be considered as a thin-walled nozzle, whose flow lines will continuously shrink when water is ejected from the nozzle [17]. Thus, no pressure has lost along the way. On the contrary, the nozzle will be defined as an elongated nozzle if its length-diameter ratio is between 2 and 4, and there is no significant difference on the velocity and flow of water jet [4]. In this case, Coanda effect, the tendency of a fluid jet to be attracted to a nearby surface, will be dominated, and in this case, we should take the pressure loss into account.

It is well accepted that the nozzle flow resistance is mainly decided by nozzle convergence angle α . The larger the convergence angle (NCA) is, the larger resistance is, and the work range of water jet is shorter in this case [20]. On the contrary, Coanda effect will take place when the nozzle convergence angle is small, and the water jet will be more unstable for obvious breakup and entrainment [17]. A study showed that

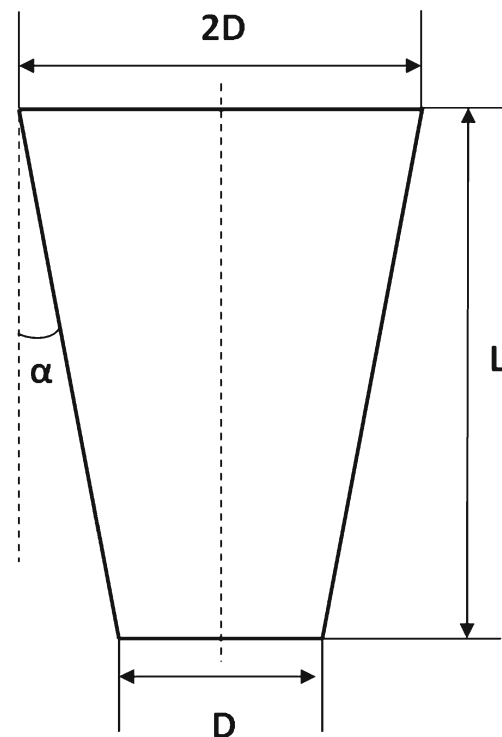


Fig. 2 The geometry of the nozzle

the water jet will be more stable when nozzle convergence angle is between 10° and 13° [4], so the NCA around 13° is selected in the following research.

Based on the grid meshing theories [21–23], the size of the nozzle (30 μm in diameter) is the smallest domain that needs to be meshed in jet meshing; however, the range of water jet (150 mm) is much larger than the nozzle. Thus, the width of the model is an important factor to be considered: millions of grids will be generated if the meshes are too small, which result in simulation burden. Conversely, larger grids will have unpredictable impact on simulation accuracy.

As showed in Fig. 3, the most important area that reveals jet flow status is around the center line of the model in jet meshing case, so this region needs to be meshed as finer grids as possible in order to obtain accurate results. On the other hand, the area far from the center line is less sensitive to flow gradient, thus ratio meshing is used to decrease the total number of grids. Hence, the region around the center line (30 $\mu\text{m} \times 6 \times 10^4 \mu\text{m}$) is meshed into the minimum grids (3 $\mu\text{m} \times 5 \mu\text{m}$), and other simulation areas are meshed by a ratio meshing method in order to make sure that the total number of grids is below 5 million.

In a 30- μm -diameter water-jet case, many meshes with different widths have been built and tested, and when the grid size of the jet exit plane is 3 μm , repeatable results are finally achievable in the 1000- μm -width mesh model with the mesh independent study (not included here due to page limit).

4 Define critical velocity and stable length

Critical Reynolds number is the parameter to classify laminar flow and turbulent flow; however, the exact critical Reynolds number is still uncertain in jet. In the year of 2000, Chen M. Y. [12] carried out an experimental and numerical study in laminar impinging slot jet flows, and he supposed that laminar flow can be achieved below 690 Reynolds numbers; then, Chiriac V. A. [13] has computed the steady and unsteady flow Reynolds number, and he thought that the flow was steady when the Reynolds number is below 750 in the year of 2002; And Gohil T. B. [24] made a conclusion that “the critical Reynolds number of jet instability purely arising due to numerical noise (discretization and round-off errors) is expected to lie between Reynolds numbers of 900 and 925” in the year of 2012. Thus, Reynolds number of 900 has been selected as the critical Reynolds number in the following work. However, the actual critical Reynolds number for a 30- μm -diameter nozzle jet is still uncertain, and it may be different from different nozzle sizes and shapes.

Reynolds number is defined as

$$Re = V \cdot D / \nu \tag{12}$$

$$\nu = \frac{\mu}{\rho} \tag{13}$$

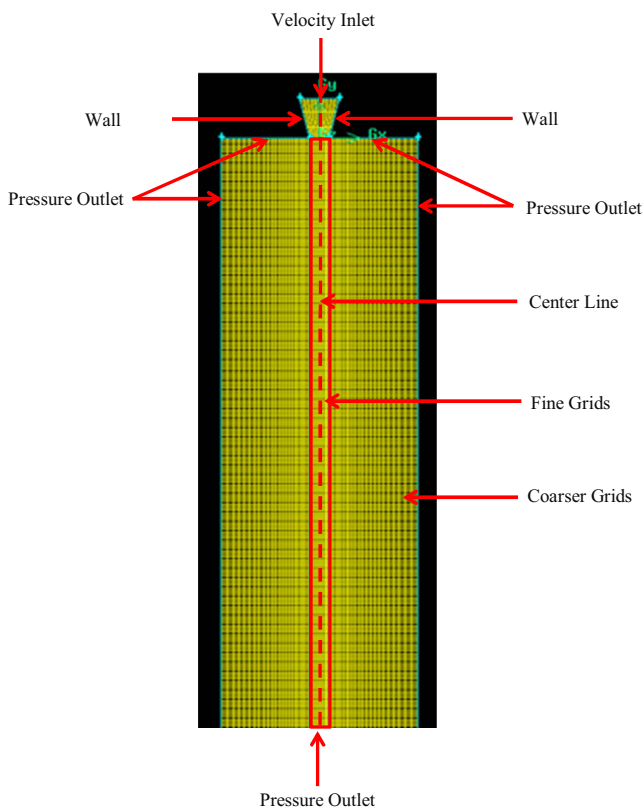


Fig. 3 The beginning part of 1000- μm -width, 6×10^4 - μm -length grid in GAMBIT

Where V and D are the velocity and diameter of water jet, respectively, and ν is the ratio of dynamic viscosity μ to the density of the fluid ρ . Normally, the kinematic viscosity of water is a constant $\nu = 10^{-6} \text{m}^2/\text{s}$ in room temperature.

So, critical velocity can be expressed as

$$V_C = 900 \cdot \nu / D = 30 \text{ m/s} \tag{14}$$

Thus, in 30- μm -diameter nozzle simulations, laminar flows are obtained if the jet exit velocity of water jet is less than 30 m/s, and vice versa. However, when the jet exit velocity is around the critical velocity (30 m/s in a 30- μm nozzle case), the flow state may be in any state of laminar, turbulence, and transition in atmospheric pressure. Thus, the 30 m/s jet exit velocity case will be simulated in both laminar and turbulence state.

Based on the computed data in FLUENT, water phase and air phase can be plotted to determine the stable jet length by the following method, which is the first time to be proposed this paper.

The acceptable unstable points (highlighted as circle in Fig. 4) are defined as the points that have slightly skew so that the laser has a slight influence with reflection to the target material. One feature of the acceptable unstable points is that the tangency angle at the acceptable points is smaller than 10° , which is set as the critical tangency angle.

On the other hand, the unacceptable unstable points (highlighted as box in Figs. 4 and 5) are those points with obvious waving shape, so that a great portion of the lasers cannot go through that point and will be reflected back to the nozzle. Other features like continuous waving, diverged jet,

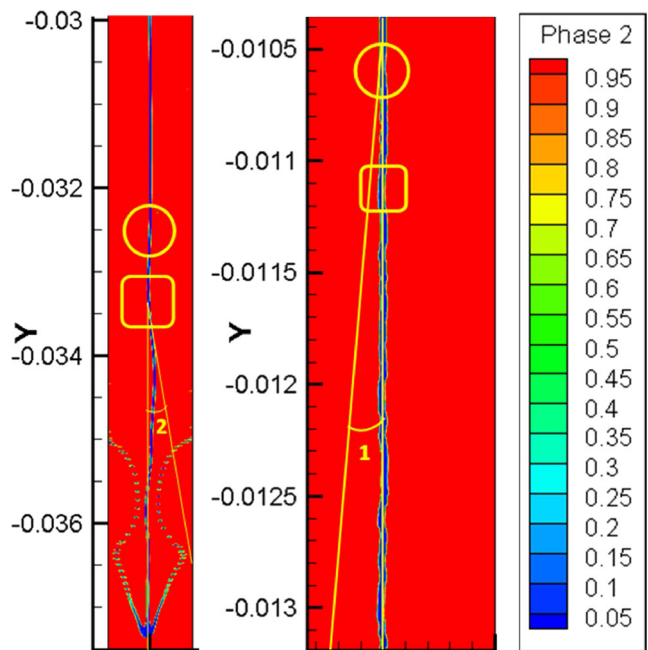
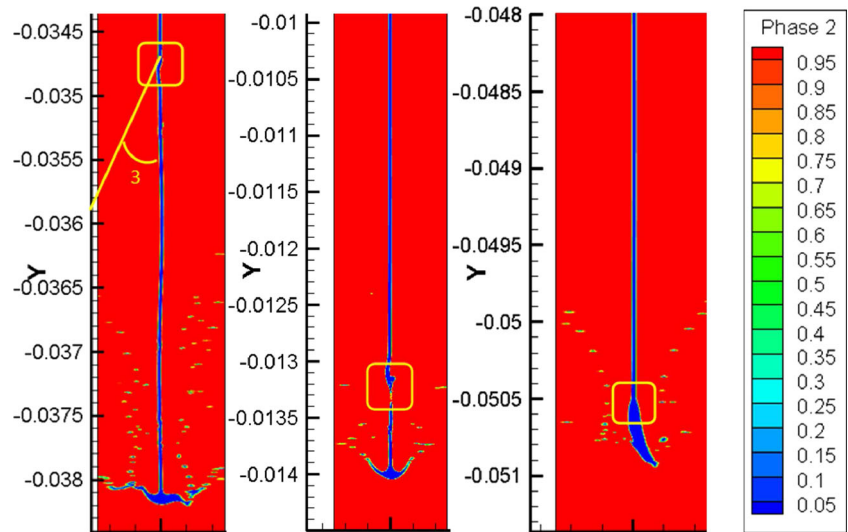


Fig. 4 Phase plots: cases with acceptable and unacceptable unstable points (y-axis is the distance to the nozzle)

Fig. 5 Phase plots: cases with the unacceptable unstable points only (y -axis is the distance to the nozzle)



breakups, and the point that the tangency angle is larger than 10° are defined as the unacceptable unstable points as well.

If there are acceptable unstable points and unacceptable unstable points in the plots,

$$L_c = (L_a + L_u) / 2 \tag{15}$$

If there is only unacceptable unstable point in the plots,

$$L_c = L_u \tag{16}$$

where L_c is the stable length of certain case, L_a is the acceptable unstable point length, and L_u is the unacceptable unstable point length judged by the critical tangency angle (10°) at that point.

Figure 4 shows the phase plots of cases with jet exit velocity 6 m/s (left) and 300 m/s (right), acceptable unstable points with a slight wave occur in both plots, and the tangency angles of both acceptable points, like the angle 1, are smaller than 10° , but the tangency angles of unacceptable unstable points in both cases, like the angle 2, are larger than 10° .

In Fig. 5, the first plot is the phase plot of 15 m/s with 0.5 air density, there is only unacceptable point that occurs around $y=0.034$ with a large wave at that point, and the tangency angle of that point, angle 3, is larger than 10° . The second plot of 120 m/s and the third one with 15 m/s with 0.001 air density have breakup and divergence point, respectively, so they are defined as the unacceptable points.

5 Results and discussion

The “mountain-like” curve of the stable length in laminar flows is observed for its maximum stable length of 0.330 m, which is more than two times of the average stable length with a velocity higher than 10 m/s in laminar flows. To be specific, the stable length of water jet rises significantly at the beginning and reaches the peak around a jet exit velocity of 6 m/s, then falls observably between 6 and 10 m/s but rather stable between 10 and 30 m/s (Fig. 6).

In the turbulence flow as shown in Fig. 7, the stable length of water-jet structure is waving around jet exit velocity 40, 100, and 280 m/s. At the beginning, the stable length of water jet has a rapidly increase between jet exit velocity 30 and 40 m/s followed by a slightly decrease between 40 and 80 m/s. Same situation takes place again around jet exit velocity 120 m/s: a significant rise (80 to 100 m/s) can be found before a small reduction between jet exit velocity of 120 and 150 m/s. Finally, the stable length of water jet is near uniform between jet exit velocity 200 and 500 m/s, after an increase between jet exit velocity 150 m/s and 200 m/s. What should be noted is that when the jet exit velocity is higher than 200 m/s and below 500 m/s, the stable length of water jet is nearly the same again and within 0.0165 m, which is the maximum stable length in turbulence simulations.

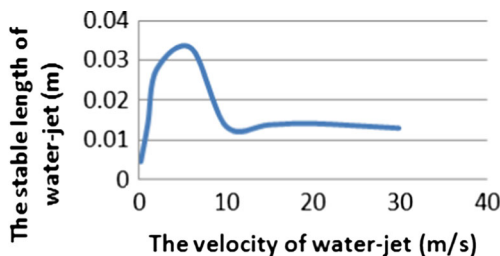


Fig. 6 The stable length curve of laminar flow

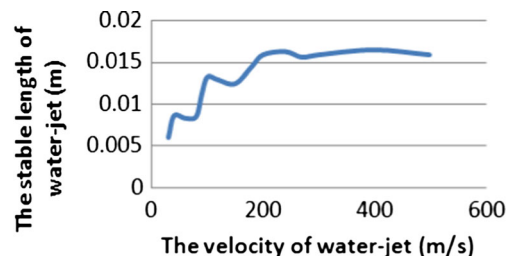


Fig. 7 The stable length curve of turbulence flow

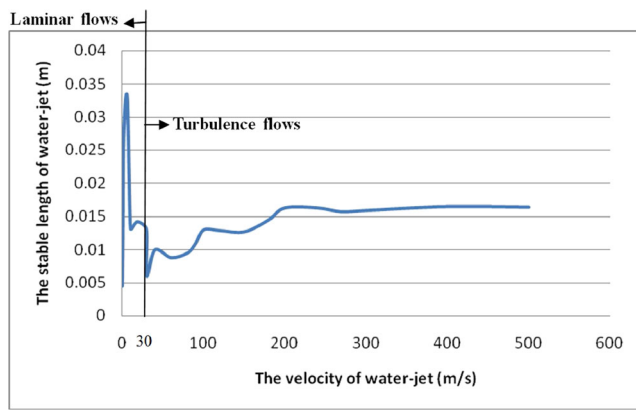


Fig. 8 The stable length curve of laminar flow and turbulence flows

Based on Fig. 8, which plots all cases in laminar and turbulence flows, it is obvious that the case that has the longest stable length is in the laminar flow, that is of more than two times of the longest stable length in turbulence flows. The most stable length (longest) is achieved around a jet exit velocity of 6 m/s in laminar flow instead of a jet exit velocity 150 to 250 m/s in turbulence flow, which are widely reported by former researchers [3, 10, 12].

Furthermore, the uncertainty at critical velocity remains with the critical Reynolds number of 30- μm -diameter nozzle case, there is no research that has verified the critical Reynolds number of a 30- μm -diameter nozzle in practical experiments. Thus, the stable length at a jet exit velocity of 29.9 m/s is presented with the stable length at 30 m/s in laminar, and the stable length at a jet exit velocity of 30.1 m/s is presented with the stable length at 30 m/s in turbulence. In the turbulence flows, the case with the longest stable length is the case with a jet exit velocity of 400 m/s. However, the stable length from 200 to 500 m/s is rather uniform and very close to the longest stable length. Although the critical velocity is uncertain, it has no effect on the data far from the critical velocity line. Hence, it is confirmed that the case with the longest stable length in laminar flow is the case with a jet exit velocity of 6 m/s.

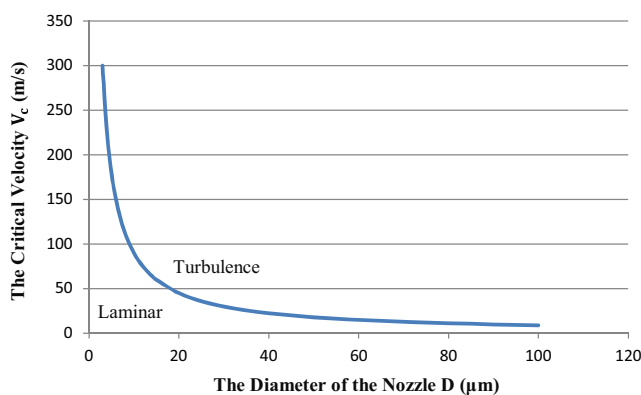


Fig. 9 The relationship between critical jet exit velocity and nozzle diameter in room temperature

Table 2 The stable length of water jet in different degrees of vacuum

Air density (kg/m ³)	Stable length (m)
1.225	0.01385
0.5	0.0348
1×10^{-5}	0.0505

At last, given that the simulation results of the cases with jet exit velocity around the critical velocity is not reliable, more experiments are needed to verify the result. Moreover, the range of velocity in a 30- μm -diameter nozzle case is large (0.2 to 500 m/s), simulation with all different velocities is impossible, so there might be an optimal velocity with longer stable length, but it will be close to the longest stable length found at 6 m/s.

Since the nozzle diameter used here is 30 μm only, laminar case can be achieved in a relative larger range of jet exit velocity (0 to 30 m/s). Based on the simulated results of a 30- μm diameter nozzle, it is supposed that the critical velocity V_c increases with a smaller exit diameter of nozzle, as shown in Fig. 9. If we have a 15- μm nozzle, its critical velocity will be around 60 m/s theoretically, but the relationship of V_c and D is otherwise; thus, more refined studies need to be conducted.

In vacuum situations, 15 m/s case with a shorter stable length was selected, in case of other cases with longer stable length will extend to the model in vacuum. By changing the density of air in FLUENT’s material settings to mimic vacuum environment, three simulations with different degrees of vacuum are done as presented in Table 2.

The results presented in Table 2 reveal that the stable length of water jet increases significantly with a vacuum environment, especially between 1.125 air density and 0.5 air density, which agrees well with the theory of jet breaking: the fraction between the water jet and air affects the jet stability. In the simulations, the stable length in the relative low vacuum environment mimicked by 0.5 kg/m³ air density is more than 2.5 times than the stable length in atmosphere conditions. Besides, the longest stable length in the high vacuum environment mimicked by 1×10^{-5} kg/m³ air density is more than 3.5 times of the stable length of the case in atmospheric pressure and around 1.45 times of the longest stable length in the relatively low vacuum environment mimicked by 0.5 kg/m³ air density.

6 Conclusion

If the critical Reynolds number of a 30- μm -diameter nozzle jet is around 900 in room temperature, it is easier to obtain stable jet in a laminar flow than turbulence flow in atmosphere. Moreover, the longest stable length in laminar flow (obtained around a jet exit velocity of 6 m/s) is more than two

times of the longest stable length in turbulence flow in atmosphere, so the jet exit velocity should be selected around 6 m/s to achieve a laminar flow so as to benefit the laser-jet coupling and machining performance in water jet-guided laser process.

The relationship between nozzle diameter and the critical velocity is plotted in Fig. 9 based on Eqs. (12), (13), and (14), and the critical velocity V_C increases significantly when the diameter of nozzle D decreases, especially when $D < 20 \mu\text{m}$. Thus, a conjecture was proposed as a future work: the smaller the diameter of the nozzle is, the more opportunity to obtain the optimal jet velocity in a laminar flow.

Contrasting with the stable length of the case with a jet exit velocity of 15 m/s in atmosphere, the vacuum plays a dramatic role in increasing the stable length of the jet. However, the stable length grows slowly between the vacuum environments mimicked by 0.5 and $1 \times 10^{-5} \text{kg/m}^3$ air density, so the vacuum environment in this range is recommended for high jet stable length.

References

- Li CF, Johnson DB, Kovacevic R (2003) Modeling of water-jet guided laser grooving of silicon. *Int J Mach Tools Manuf* 43(9): 925–936
- Porter JA, Louhisalmi YA, Karjalainen JA, Fuger S (2007) Cutting thin sheet metal with a water jet guided laser using various cutting distances, feed speeds and angles of incidence. *Int J Adv Manuf Technol* 33(9–10):961–967
- Perrottet D., Amorosi S., and Richerzhagen B. (2005) New process for screen cutting: water-jet guided laser, Proceedings of SPIE, the International Society for Optical Engineering. Society of Photo-Optical Instrumentation Engineers: 596105.1-596105.5
- Ye R. F. (2009) The key technology and optical system of water-jet guided laser machining. Diss. (Ph.D), Xiamen University
- Richerzhagen B (1997) Water guided laser processing. *Indust Laser Rev* 11:8–10
- Zhan C. J., Li C. F., Wang Y. L., Liu T., Pan Y. C. (2010) Numerical study of water-jet guided laser drilling of silicon based on FVM. AIP Conference Proceedings, Vol. 1233
- Perrottet D., Green S., and Richerzhagen B. (2006) Clean dicing of compound semiconductors using the water-jet guided laser technology, IEEE/SEMI Advanced Semiconductor Manufacturing Conference: 233–236
- Perrottet D., Housh R., Richerzhagen B., and Manley J. (2005) Heat damage-free laser-microjet cutting achieves highest die fracture strength, lasers and applications in science and engineering. *Int Soc Optics Photonics*: 285–292
- Sibailly O. D., Wagner F. R., Mayor L., and Richerzhagen, B. (2003) High precision laser processing of sensitive materials by microjet, Fourth International Symposium on Laser Precision Microfabrication. International Society for Optics and Photonics: 501–504
- Perrottet D., Spiegel A., Wagner F. R., Housh R., Richerzhagen B., and Manley J. (2005) Particle-free semiconductor cutting using the water jet guided laser, *Lasers and Applications in Science and Engineering*. International Society for Optics and Photonics: 240–246
- Lee HG, Yoon HS, Ha MY (2008) A numerical investigation on the fluid flow and heat transfer in the confined impinging slot jet in the low Reynolds number region for different channel heights [J]. *Int J Heat Mass Transf* 51(15):4055–4068
- Chen MY, Chalupa R, West AC, Modi V (2000) High Schmidt mass transfer in a laminar impinging slot jet flow [J]. *Int J Heat Mass Transf* 43(21):3907–3915
- Chiriac VA, Ortega A (2002) A numerical study of the unsteady flow and heat transfer in a transitional confined slot jet impinging on an isothermal surface. *Int J Heat Mass Transf* 45(6):1237–1248
- Shanmugam DK, Nguyen T, Wang J (2008) Effect of liquid properties on the stability of an abrasive water-jet. *Int J Mach Tools Manufact* 48(10):1138–1147
- Yan CJ, Xie MZ (2008) Effect of aerodynamic force on the breakup behavior of jets. *J Eng Math* 25(3):564–566
- Söderberg LD, Alfredsson PH (1998) Experimental and theoretical stability investigations of plane liquid jets. *Euro J Mech-B/Fluids* 17(5):689–737
- Lin JZ, Ruan XD, Chen BG (2005) *Hydromechanics*. Tsinghua University Press, Beijing
- Wang HZ (2008) The theory and applications of micro water-jet guided laser machining. *Equip Electron Prod Manufact* 158:27–31
- Su H. X. (1998) The water-jet guided laser machining. *Optoelectronic technology & information*.11.003: 35–38
- Xu R, Du C I, Zeng R, Zhang JJ (2011) Study on jet simulation of nozzles with different contraction angles. *J Min Mach* 39(2):36–39
- Zhang DY, Luo YH, Li X, Chen HW (2011) Numerical simulation and experimental study of drag-reducing surface of a real shark skin. *J Hydrodyn* 23(2):204–211
- Luo YH, Liu YF, Zhang DY, Ng EYK (2014) Influence of morphology for drag reduction effect of sharkskin surface. *J Mech Med Biol* 14(2):1450029–1–1450029–16
- Gong WJ, Wang JM, Gao N (2011) Numerical simulation for abrasive water jet machining based on ALE algorithm. *Int J Adv Manuf Technol* 53(1–4):247–253
- Gohil TB, Saha AK, Muralidhar K (2012) Numerical study of instability mechanisms in a circular jet at low Reynolds numbers. *Comput Fluids* 64:1–18